Cationic Polystyrene Nanosphere Toxicity Depends on Cell-Specific Endocytic and Mitochondrial Injury Pathways. ACS Nano

ARTICLE *in* ACS NANO · FEBRUARY 2008

Impact Factor: 12.88 · DOI: 10.1021/nn700256c · Source: PubMed

Cationic Polystyrene Nanosphere Toxicity Depends on Cell-Specific Endocytic and Mitochondrial Injury Pathways

Tian Xia,[†,#] Michael Kovochich,[†,#] Monty Liong,[‡] Jeffrey I. Zink,[‡,⊥] and Andre E. Nel[†,§,⊥,*]

[†]Division of NanoMedicine, Department of Medicine, [‡]Department of Chemistry & Biochemistry, [§]The Southern California Particle Center, and [⊥]California NanoSystems Institute, University of California, Los Angeles, California 90095. [#]These authors contributed equally to this work.

ABSTRACT The exponential increase in the number of new nanomaterials that are being produced increases the likelihood of adverse biological effects in humans and the environment. In this study we compared the effects of cationic nanoparticles in five different cell lines that represent portal-of-entry or systemic cellular targets for engineered nanoparticles. Although 60 nm NH_2-labeled polystyrene (PS) nanospheres were highly toxic in macrophage (RAW 264.7) and epithelial (BEAS-2B) cells, human microvascular endothelial (HMEC), hepatoma (HEPA-1), and pheochromocytoma (PC-12) cells were relatively resistant to particle injury. While the death pathway in RAW 264.7 cells involves caspase activation, the cytotoxic response in BEAS-2B cells is more necrotic in nature. Using fluorescent-labeled NH_2-PS, we followed the routes of particle uptake. Confocal microscopy showed that the cationic particles entered a LAMP-1 positive lysosomal compartment in RAW 264.7 cells from where the particles could escape by lysosomal rupture. A proton pump inhibitor interfered in this pathway. Subsequent deposition of the particles in the cytosol induced an increase in mitochondrial Ca^{2+} uptake and cell death that could be suppressed by cyclosporin A (CsA). In contrast, NH_2-PS toxicity in BEAS-2B cells did not involve the LAMP-1 endosomal compartment, stimulation of proton pump activity, or an increase in mitochondrial Ca^{2+}. Particles were taken up by caveolae, and their toxicity could be disrupted by cholesterol extraction from the surface membrane. Although the particles induced mitochondrial damage and ATP depletion, CsA did not affect cytotoxicity. Cationic particles were taken up into HEPA-1, HMEC, and PC-12 cells, but this did not lead to lysosomal permeabilization, increased Ca^{2+} flux, or mitochondrial damage. Taken together, the results of this study demonstrate the importance of cell-specific uptake mechanisms and pathways that could lead to sensitivity or resistance to cationic particle toxicity.

KEYWORDS: cationic nanoparticle · nanotoxicology · endocytosis · mitochondria · cell death

Because of the rapid growth in the nanotechnology industry, a large number of novel engineered nanomaterials (NMs) are being produced and introduced to the marketplace.[1] This increases the likelihood that workers in the nanotechnology industry, consumers, and ultimately the environment could come into contact with these materials. Because of their small size, large surface area, surface reactivity, chemical composition, and other unique physicochemical properties, engineered nanoparticles (NPs) are capable of interacting with biological components or systems, many of which are nanoscale operations.[1] It is not a surprise, therefore, that academia, government, industry, and members of the public have expressed great concern about the possibility that engineered NMs could lead to adverse biological effects in humans and the environment. In fact, these concerns have led to the establishment of a new science, nanotoxicology, which aims to understand the physicochemical principles and biological pathways by which engineered NMs could lead to adverse biological outcomes. This information is key toward developing screening assays, risk assessment, exposure assessment, dose calculations, and formulation of regulatory policy.[1–6]

Some of the leading paradigms that have emerged as potential predictors of biological injury include the ability of semiconductor materials, metal oxides, and metal contaminants to generate reactive oxygen species (ROS) and oxidant injury.[1,7] However, oxidant injury is by no means the only paradigm for injury, and material characteristics that contribute to cellular uptake, subcellular localization, and interaction with biomolecules need to be considered.[1] Such material characteristics include NP size, hydrophobicity, surface charge, and surface coatings; these are key determinants for particle binding and wrapping by the surface membrane as well as defining the possible route of endosomal uptake. These are principles to keep in mind during the development of biological assays that can be used to screen for the potential bioadverse effects of NMs. These screening platforms could allow us to develop a

*Address correspondence to anel@mednet.ucla.edu.

Received for review September 25, 2007 and accepted November 29, 2007.

Published online December 27, 2007.
10.1021/nn700256c CCC: $40.75

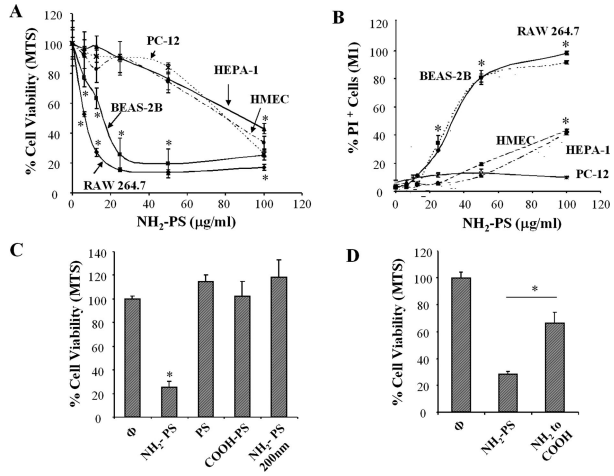

Figure 1. Cell viability/death detection by the MTS assay and PI staining. (A) After stimulation with NH_2-PS particles at doses of 6–100 μg/mL for 16 h, cells were incubated with the MTS reagent for 30 min, and the absorbance was measured at 490 nm. All the MTS values of different doses were normalized according to the control values (no particle exposure), which were regarded as 100% cell viability. (B) Similar to the experiment in A, during which cells were stained with 47.5 μg/mL PI and immediately analyzed by flow cytometry. The percentage of PI-positive (M1-gated) cells was scored by Cellquest, as shown in Figure S1. (C) After overnight stimulation of RAW 264.7 cells with 25 μg/mL of the different types of PS nanospheres, cell viability was determined using the MTS assay. In order to show the critical effects of size, we also included a 200 nm NH_2-PS particle. (D) The NH_2 group on the nanospheres was changed to COOH, whereupon the RAW 264.7 cells were treated with 25 μg/mL of each particle type before performance of the MTS assay. *$p < 0.01$ compared with control. Data are representative of three separate experiments with at least three wells per treatment.

more rapid assessment of materials that are potentially hazardous or potentially safe.[1,8] This could assist in prioritizing which materials should be studied in more depth. Without the availability of predictive toxicological assays, our ability to provide safety assessments for the large number of emerging NMs could prove to be an overwhelming task. Thus, nanotechnology should try to avoid the conundrum faced by the chemical industry where only a few hundred of more than 40 000 industrial chemicals have undergone toxicity testing. Due to this backlog, we are faced with new forms of chemical toxicity on an annual basis.

In our own attempts to develop predictive toxicology approaches to NM testing, we have previously demonstrated that cationic polystyrene (PS) nanoparticles with an NH_2 attachment to their surfaces are associated with a high rate of toxicity in macrophages.[9] Cationic particle toxicity at the cellular level could translate into clinical toxicity, as evidenced by the development of acute pulmonary edema in textile paint sprayers that are exposed to polycationic paint particles.[10,11] Moreover, it has been demonstrated that the same polycationic paint polymers induce pulmonary injury in hamsters and rats after tracheal instillation or inhalation exposure.[10,11] Similarly, it has been demonstrated that NH_2-PS nanospheres induce pulmonary inflammation and thrombosis in hamsters, while naked or COOH-modified PS had little or no effect.[11] Polycationic NPs can also induce rapid bacterial clearance from a growth medium, implying that the release of these materials into the environment could also lead to adverse ecological consequences.[12] Thus, although NH_2-PS does not represent an actual commercial product that is likely to lead to real-life exposures, the availability of these experimental particles represents an important tool for understanding cationic NP toxicity.

>In this article, we dissect the mechanism of the NH_2-PS cytotoxicity as a paradigm for cationic NP injury. It has previously been suggested that the cellular uptake of cationic particles into a lysosomal compartment could lead to cytotoxicity by effects on the acidifying proton pump.[13] According to the proton sponge hypothesis, polyamine groups with high proton binding affinity could lead to buffering and exaggerated proton pump activity. This toxicity is thought to result from chloride influx to maintain charge neutrality, thereby leading to osmotic swelling and rupture of the lysosome.[14] Indeed, an endosomal escape strategy is widely used for plasmid, DNA, and drug delivery; these carrier systems are specifically designed to be sensitive to the luminal pH of the endosomes. In addition to effects on lysosomal function, cationic molecules have also been shown to target cell membranes through strong binding to phospholipid components, which can lead to membrane disruption or fusogenic activity.[15]

To study cationic particle toxicity in mammalian cells, we used fluorescent labeling and cellular imaging to follow the cellular fate of the NH_2-PS nanospheres in five different cell lines, namely a macrophage (RAW 264.7) and epithelial (BEAS-2B), hepatocyte (HEPA-1), endothelial (HMEC), and pheochromocytoma (PC-12) cell lines. We demonstrate differential cellular uptake pathways that could be engaged in cell-specific injury *via* mechanisms such as lysosomal rupture, intracellular calcium flux, and mitochondrial injury.

RESULTS

Differential Toxicity of NH_2-PS Nanospheres in Different Cell Types. We have previously shown that cationic PS nanospheres exert toxic effects in the macrophage cell line, RAW 264.7.[9] In order to compare this to the possible toxic effects of NH_2-PS in bronchial epithelial (BEAS-2B), hepatoma (HEPA-1), human microvascular endothelial (HMEC), and pheochromocytoma (PC-12) cells, the cultures were co-incubated with increasing amounts of the particles for different lengths of time (1–16 h), followed by performance of the MTS assay. Cell viability was expressed as the percent dehydrogenase activity compared to that of untreated control cells (100% viability). Figure 1A demonstrates a clear and dose-dependent decrease in MTS activity in RAW 264.7 and BEAS-2B cells after 16 h, while PC-12, HEPA-1, and HMEC showed a significant decline in cell viability only at

doses >50 μg/mL (Figure 1A). These differences are reflected by comparing the IC_{50} values of the particles in three separate experiments: RAW 264.7 = 8.2, BEAS-2B = 12.1, HEPA-1 = 84, HMEC = 86, and PC-12 = 90 μg/mL. We confirmed that the decline in MTS activity represents actual cell death, as determined by increased propidium iodide (PI) uptake (Figures 1B and S1). Figure S2A shows a time-dependent decrease in MTS activity in RAW 264.7 and BEAS-2B cells.

In order to confirm that the observed toxic effects are linked to the NH_2 substitution on the particle surface, two different approaches were used. First, we compared NH_2-PS with carboxy-labeled (COOH-PS) and non-labeled (PS) nanospheres. This demonstrated that only 60 nm NH_2-PS but not similarly sized PS or COOH-PS particles could induce decreased MTS activity (Figure 1C). Primary particle size is important in this assay since 200 nm NH_2-PS microspheres were inactive (Figure 1C); this was true for a dose up to 200 μg/mL. Similar results were obtained in BEAS-2B cells (not shown). In the second approach, the amine groups were modified to carboxylate groups before toxicity testing (Figure 1D). This chemical transition leads to a significant reversal of particle toxicity (Figure 1D). In order to see if the toxicity of the NH_2 group can be caused by other cationic groups, we used 60 nm PS particles that contained an amidine [$R_nC(=NH)NH_2$] attachment. Although this induced significant toxicity in RAW 264.7 cells, the level of cell damage was decreased compared to that observed with NH_2-PS (Figure S2B). The reduced level of toxicity could relate to the relatively high rate of proton saturation of the amidine group.

In order to determine whether the decrease in cell viability in RAW 264.7 and BEAS-2B cells is due to caspase activation or DNA cleavage, D2R trifluoroacetate was used to assess caspase activation in the hydrolysis of the fluorescent substrate (Figure S3A), while DyeCycle Orange was used to assess the generation of hypodiploid DNA (Figure S3C).[16] Interestingly, while NH_2-PS nanospheres induced an increase in the percentage of RAW 264.7 cells showing caspase activation and hypodiploid DNA, there was a relative paucity and slow onset of similar events in BEAS-2B cells (Figure 2A,B). In order to determine whether these results reflect different mechanisms of cytotoxicity, we also looked at mitochondrial events that are often associated with the onset of cell death. This was determined by studying JC-1 fluorescence to assess the percentage of cells in the population with decreased mitochondrial membrane potential ($\Delta\Psi_m$) (Figure S3B) as well as measuring cellular ATP content. While cationic NPs induced a dramatic decline in cellular ATP content in both cell types, there was a more dramatic and faster rate of $\Delta\Psi_m$ decline in RAW 264.7 cells (Figure 2C,D). All considered, these changes are compatible with an apoptotic process in RAW 264.7, while BEAS-2B cells failed to exhibit evidence of caspase activation or DNA cleavage. Moreover, the decrease in cell viability and ATP content in BEAS-2B cells, together with the features of perinuclear clustering of mitochondria and intracellular calcium overload that will be discussed later, is more suggestive of necrotic cell death. HEPA-1, HMEC, and PC-12 cells were relatively resistant to the effects of NH_2-PS (Figure 1A) and showed little or no change in caspase activation, DNA cleavage, $\Delta\Psi_m$, and ATP content (Figure S4).

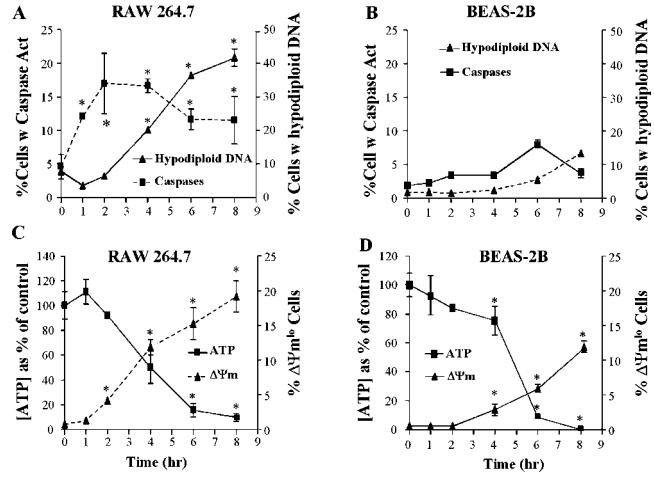

Figure 2. Elucidation of the mechanism of cytotoxicity using assays for caspase activation, DNA cleavage, mitochondrial membrane potential ($\Delta\Psi_m$), and cellular ATP content. After the cells were stimulated with 25 μg/mL of NH_2-PS for 1, 2, 4, 6, and 8 h, the above cellular responses were assayed as described in the Materials and Methods and Supporting Information (Figure S3). Caspase activation, DNA degradation, and $\Delta\Psi_m$ decline were expressed as the percentage of cells in the population showing the indicated changes (see Figure S3). Cellular ATP content was expressed as a percentage of the ATP content of control cells, which was regarded as 100%. *$p < 0.01$ compared with control. Data are presented from three separate experiments.

Cellular Uptake, Subcellular Processing, and Toxicity of Fluorescent-Labeled NH_2-PS Nanoparticles. We have previously hypothesized that the cytotoxic effect of cationic PS nanospheres could involve lysosomal rupture in RAW 264.7 cells.[9] According to the proton sponge hypothesis, polyamine groups with a high buffering capacity lead to exaggerated proton pump activity that will otherwise be shut down by an increase in acidity.[9,13] Due to the concomitant Cl^- uptake to maintain electro-neutrality, it has been proposed that osmotic swelling leads to rupture of the endocytic vesicles and particle deposition in the cytosol.[14] In order to study lysosomal rupture, the NH_2-PS nanospheres were FITC labeled (FITC-NP) to follow their intracellular fate. Although fluorescence labeling leads to a minor increase in particle aggregation, as demonstrated by transmission electron microscopy (TEM, Figure S5A) and light scattering (Table 1), this effect was negated by the inclusion of fetal calf serum (FCS) proteins in the complete medium (Table 1). When compared against the non-labeled particles, there was a small but significant reduction in the level of toxicity in RAW 264.7 cells (Figure 3A). This effect was even more accentuated in BEAS-2B cells (Figure S6). A possible explana-

TABLE 1. Physical Characterizations and IC_{50} of the Nanospheres[a]

particle type	aqueous → DMEM size (nm)	PDI	zeta potential	RAW cells IC_{50} (μg/mL)
NH_2-PS, 60 nm	63 → 415	0.120 → 0.284	+35.8 → −3.7	8.2
FITC-NH_2-PS, 60 nm	332 → 306	0.301 → 0.284	−0.27 → −26.65	14.6
amidine-PS, 70 nm	71 → 319	0.045 → 0.347	+45.6 → −4.9	34.5
NH_2-PS, 200 nm	297 → 250	0.195 → 0.205	+5.61 → −11.0	not toxic

[a]Particle size distribution and zeta potential were measured using a ZetaPALS as described in the Materials and Methods. The reported mean particle size (average diameter) is calculated on the basis of an intensity-weighted average. PDI is the polydispersity index. IC_{50} was determined using the MTS cell viability assay as described in the Materials and Methods. DMEM = Dulbecco's Modified Eagle Medium.

tion is that FITC labeling affects the zeta potential of the particle, but not to the extent that it changes all the available NH_2 groups (Table 1). However, at acidification levels (pH < 4) that can be achieved in the lysosomal compartment, it is interesting that the particles regain a positive charge (Figure S5B). This could influence particle toxicity in cells that utilize this uptake route (see later). FITC-NP did not exert toxic effects in HMEC, PC-12, or HEPA-1 cells (not shown).

Studying cellular fluorescence in a flow cytometer was done initially to follow cellular uptake of the labeled particles. This showed both a time- (not shown) and dose-dependent increase (Figure 3B) in mean fluorescence intensity (MFI) compared to the non-particle-treated controls. While the magnitudes of increase in RAW 264.7, HEPA-1, HMEC, and PC-12 cells were comparable, BEAS-2B cells displayed a proportionally larger increase in fluorescent intensity (Figure 3B). We also followed the intracellular location of the fluorescent particles by confocal microscopy. First, we assessed FITC-NP uptake in RAW 264.7 cells in combination with Alexa 594 staining to detect the expression of the lysosomal protein, LAMP-1. Merging of the red and green fluorescence profiles revealed considerable co-localization of the particles with LAMP-1 (as demonstrated by the composite yellow fluorescent staining pattern in Figures 4A and S7). Scoring of the degree of overlap by Image J software showed that the percentage of particles co-localizing with LAMP-1 decreased from 84% to 65% to 23% at 2, 4, and 6 h, respectively (Figure 4B). Moreover, the appearance of the fluorescent intracellular particles changed from predominantly small yellow fluorescent spots at 2 h to a mixed population of small and large, mostly green fluorescent spots at 6 h (Figure 4A). These data are compatible with a time-dependent change in the subcellular localization of the particles. In order to determine that the fluorescence is indeed particle related, we also looked at the staining pattern in RAW 264.7 cells that were treated with FITC alone. This did not reveal any fluorescence uptake, which, together with dialysis procedures showing that the FITC group does not dissociate from the particle surface in cell culture medium, helps to confirm that the cellular fluorescence obtained with FITC-NP is likely particle associated.

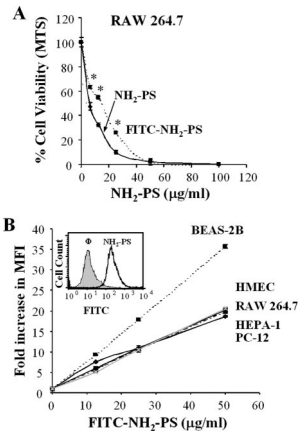

Figure 3. Cellular uptake and cytotoxicity of FITC-labeled NH_2-PS nanospheres. NH_2-PS nanoparticles were FITC labeled as described in the Materials and Methods. (A) Cytotoxicity of NH_2-PS before and after FITC labeling was compared in RAW 264.7 cells using the MTS assay. These cells were exposed to the indicated dose of the particles for 16 h. Data are representative of three separate experiments. *p < 0.01 compared with NH_2-PS. (B) Dose-dependent particle uptake as determined by flow cytometry. The inset is a representative histogram showing the shift in fluorescence intensity in RAW 264.7 cells treated with 25 μg/mL FITC-NH_2-PS for 4 h. The fold-increase in fluorescent intensity was calculated and used to generate the graph, in which all cell types were compared over the dose range shown.

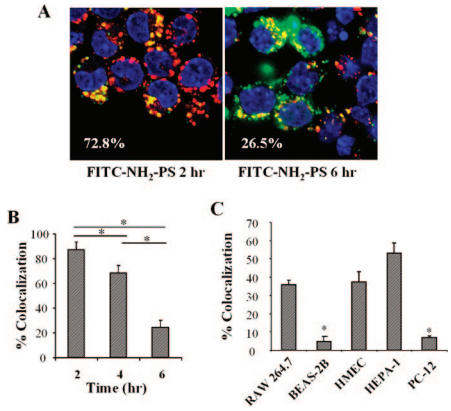

Figure 4. Confocal microscopy to study the subcellular localization of FITC-labeled NH_2-PS nanospheres. (A) RAW 264.7 cells were treated with 25 μg/mL FITC-NH_2-PS for 2–6 h. After fixation and permeabilization as described in the Materials and Methods, cells were stained with the lysosomal marker LAMP-1 and visualized using a Lecia 1P-FCS confocal microscope. The red and green fluorescent images that correspond to the merged panel on the left-hand side are shown in Figure S7. After merging, the percentage of particles that are co-localized with LAMP-1 (yellow fluorescent pattern) was quantified by Image J. (B) The percent co-localization was calculated in three separate experiments, each of which examined at least six separate fields. *p < 0.01. (C) Triplicate experiments and assessment of co-localization were performed in all five cell types after incubation with FITC-NH_2-PS for 6 h. Co-localization was scored as above.

Similar experiments were conducted in other cell types, which also show a time-dependent increase in particle uptake but with varying degrees of overlap

with LAMP-1 (Figures 4C and S8). Thus, while HMEC and HEPA-1 cells showed a relatively high degree of merging with LAMP-1, the extent of co-localization was much less in BEAS-2B and PC-12 (Figure S8). These differences were reproduced in three separate experiments and shown to be statistically significant ($p < 0.01$) when comparing RAW 264.7 (33%), HEPA-1 (51%), and HMEC (46%) data to those of either BEAS-2B (8%) or PC-12 (7%) (Figure 4C). Interestingly, no change occurred wherein the yellow changed to a predominant green fluorescent pattern in HEPA-1 and HMEC cells (not shown). All considered, these data suggest different routes of uptake and intracellular processing of particles in different cell types.

NH_2-PS Nanoparticles Induce Lysosomal Permeabilization and Toxicity That Can Be Reversed by Bafilomycin A1 (BFA) in RAW 264.7 Cells. A more direct demonstration of the ability of cationic PS nanoparticles to induce lysosomal permeabilization was sought using the lysosomotropic dye, acridine orange (AO). AO uptake in acidic lysosomes leads to red fluorescence, which dissipates when the dye leaves this compartment. The accompanying decrease in fluorescence intensity can be followed by flow cytometry, which allows scoring of the percentage of AO^{low} cells as an index of lysosomal permeabilization (Figure S9A). While it could clearly be demonstrated in RAW 264.7 cells that their lysosomal permeabilization is both time- (Figure 5A) and dose-dependent (Figure S9B), no permeabilization could be observed in any of the other cell types (Figure 5A). This suggests that lysosomal permeabilization plays a key role in NH_2-PS toxicity in RAW 264.7 cells. This is in keeping with the confocal data showing a significant reduction of FITC-NP co-localization with LAMP-1 over time (Figure 4B).

In order to more directly demonstrate the role of the proton pump in NH_2-PS toxicity in RAW 264.7 cells, we made use of bafilomycin A1 (BFA), a v-ATPase inhibitor that prevents endosomal acidification. Two approaches were used to determine the BFA effects. First, confocal microscopy was used to assess intracellular particle localization in relation to LAMP-1 staining. This demonstrated that the drug exerted a significant effect on particle colocalization with LAMP-1 (Figure 5B). Thus, the addition of BFA increased the degree of co-localization from 39% to 65% at 6 h (Figure 5B). This effect was statistically significant in three repeat experiments (Figure 5C), indicating that inhibition of proton pump activity leads to enhanced lysosomal retention. This notion is further supported by the size of the particle aggregates and differences in the yellow and green fluorescent patterns (Figure 5B). The second experiment with BFA was to look at cellular toxicity. Using PI uptake, we demonstrated that BFA decreases NH_2-PS toxicity in a dose-dependent manner (Figure 5D). In contrast, BFA had no effect on the decreased cellular viability in BEAS-2B cells or on the intracellular localization of the labeled particles in other cell types (not shown). These data confirm the importance of a lysosomal processing pathway and the role of the proton pump in cationic particle toxicity in RAW 264.7 cells. These data also suggest a different mechanism of toxicity in BEAS-2B cells.

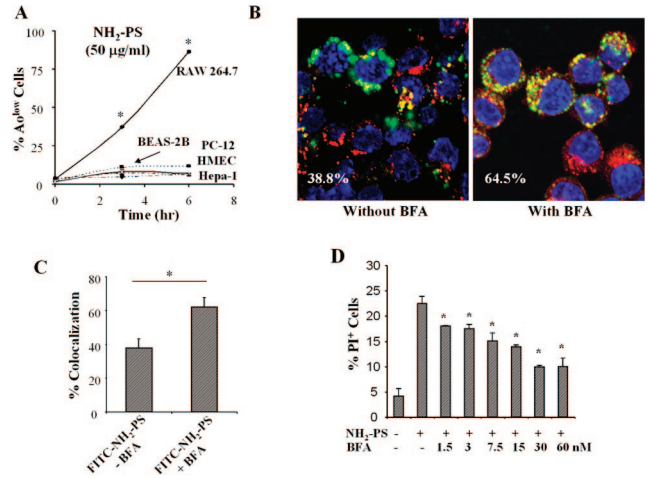

Figure 5. Assessment of particle effects on lysosomal integrity as determined by flow cytometry and confocal microscopy. (A) Assessment of lysosomal integrity by assessment of fluorescence intensity in a flow cytometer. After treatment with 25 μg/mL NH_2-PS for 3 and 6 h, cells were stained with AO and analyzed by flow cytometry to detect the population of AO^{low} cells, as shown in Figure S9. The M1-gated population was expressed as percent of total cells at 3 and 6 h. (B) Representative confocal display showing particle co-localization profile with LAMP-1 in the absence or presence of 60 nM BFA. Cells were treated with 25 μg/mL of the particles for 6 h. (C) Statistical analysis of the percent co-localization in the absence or presence of BFA in three separate experiments, in which at least six separate fields were analyzed in each experiment. *$p < 0.01$. (D) Dose-dependent protection of NH_2-PS-induced cytotoxicity in RAW 264.7 cells by BFA. Data are representative of three separate experiments.

NH_2-PS Toxicity in BEAS-2B Cells Is Dependent on Caveolar Uptake and Can Be Reversed by Methyl-β-cyclodextrin (MbCD). Although NH_2-PS nanospheres are toxic to BEAS-2B cells, there is no indication of lysosomal permeabilization, suggesting an alternative route of cellular uptake and toxicity. Caveolae have recently emerged as an important route for viral uptake that can bypass the traditional endosome/lysosome route.[17,18] In order to test this pathway, BEAS-2B cells were treated with FITC-NP, following which we stained for caveolin-1 localization with an Alexa 594-labeled antibody. Confocal microscopy demonstrated a high degree (64%) of overlap between FITC-NP and red fluorescent caveolin-1 in BEAS-2B cells (Figure 6A). In order to demonstrate that caveolae are important for cellular uptake, we used the inclusion of these structures in lipid rafts on the surface membrane to see if we can interfere in particle uptake. Caveolae can be disrupted by the sterol-sequestering agent, methyl-β-cyclodextrin (MbCD), that extracts cholesterol from the lipid rafts. Indeed, after treating BEAS-2B cells with MbCD, we confirmed by confocal imaging (Figure 6B) and flow cytometry (not shown) that lipid raft disruption leads to decreased FITC-NP uptake. Furthermore, MbCD significantly re-

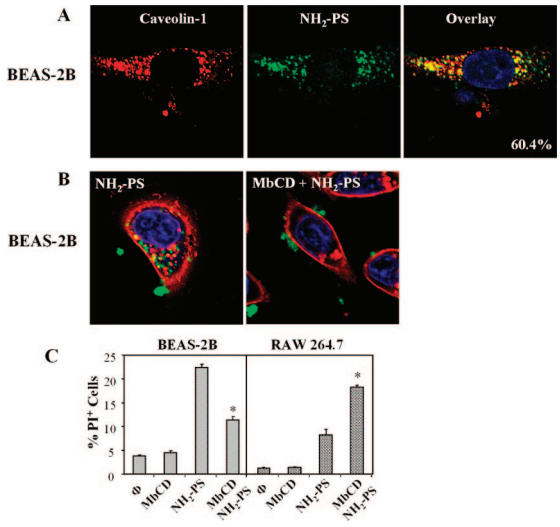

Figure 6. Particle uptake in BEAS-2B cells is dependent on caveolae and can be disrupted by cholesterol depletion. (A) Confocal microscopy to show co-localization of NH_2-PS with caveolin-1 in BEAS-2B cells. Cells were treated with 25 μg/mL FITC-NH_2-PS for 6 h before cellular preparation and staining with anticaveolin-1 Ab. Cells were examined using a Lecia 1P-FCS confocal microscope, and representative images are shown. (B) BEAS-2B uptake of FITC-NH_2-PS in the absence or presence of 1 μM MbCD. The cell membrane was stained with 5 μg/mL red fluorescent wheat germ agglutinin (WGA). (C) Comparison of NH_2-PS cytotoxicity in RAW 264.7 and BEAS-2B cells pretreated with 1 μM MbCD, before incubation with 25 μg/mL NH_2-PS for 6 h. Cellular viability was determined by PI uptake. *$p < 0.01$ compared with NH_2-PS. Data are representative of three separate experiments.

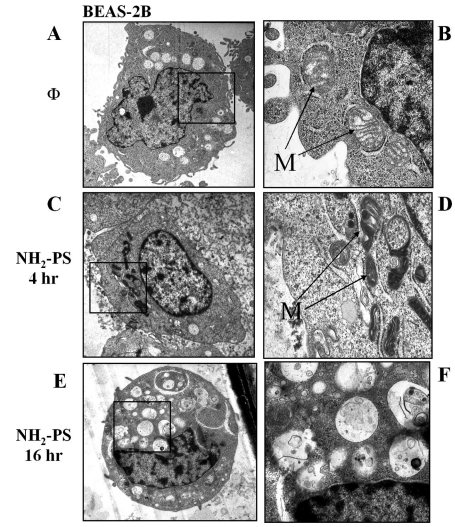

Figure 7. Electron microscopy to determine the ultrastructural changes in BEAS-2B cells after exposure to 10 μg/mL NH_2-PS for the indicated time period. Panels on the left depict magnification at 4800×, while panels on right depict magnification at 15000× to show the mitochondrial details. Notice the mitochondrial shrinkage at 4 h, followed by organellar disappearance, thereby yielding vacuolar expressing cells at 16 h. The comparison figure for RAW 264.7 cells is shown in the Supporting Information (Figure S10).

duced NH_2-PS-induced cell death in BEAS-2B cells (Figure 6C). In contrast, this drug increased particle toxicity in RAW 264.7 cells (Figure 6C).

Ultrastructural and Functional Studies Demonstrating a Key Role for Intracellular Ca^{2+} and Mitochondria in Cationic Particle Toxicity. We have previously shown that NH_2-PS nanospheres induce mitochondrial damage in RAW 264.7 cells.[9] Ultrastructural resolution by electron microscopy (EM) confirmed that the cationic particles induce early-onset (<4 h) swelling of this organelle, following which cristae disappear from structurally damaged mitochondria (Figure S10). This results in a vacuolar cellular appearance in which the appearance of myelin figures in the vacuolae suggests the mitochondrial origin (Figure S10).

EM analysis in BEAS-2B cells shows a different evolution of mitochondrial ultrastructural changes, starting with mitochondrial condensation at 4 h, before leading to structural damage and mitochondrial disappearance at 16 h (Figure 7). The mitochondrial damage can also be followed by confocal microscopy, in which these organelles are revealed by staining for complex V inhibitor protein (Figure S11A). Again, this demonstrated the disappearance and condensation of mitochondria. All considered, these ultrastructural changes suggest that the mitochondrion is a prominent target for cationic particle toxicity in RAW 264.7 and BEAS-2B cells.

No noticeable mitochondrial damage occurred in HEPA-1, PC-12, and HMEC (not shown), in keeping with the lack of toxicity in these cells (Figure 1).

Figure 2 demonstrates that cationic particles exert functional effects on mitochondria. Although there are a number of mechanisms by which cationic nanospheres could induce mitochondrial damage, one possibility is an effect on intracellular Ca^{2+} flux. Mitochondria play an important role in regulating the intracellular calcium concentration, $[Ca^{2+}]_i$, through their ability to sequester this divalent cation from the cytosol. This buffering effect could lead to an increase in mitochondrial Ca^{2+}, $[Ca^{2+}]_m$. $[Ca^{2+}]_m$ is one of the key regulators of the permeability transition pore (PTP).[19–21] $[Ca^{2+}]_i$ and $[Ca^{2+}]_m$ were assessed by looking at Fluo-3 and Rhod-2 fluorescence, respectively (Figure 8). While NH_2-PS could induce a dose-dependent increase in $[Ca^{2+}]_i$ in RAW 264.7 and BEAS-2B cells, the magnitude of the change was bigger in the former cell type (Figure 8A). In contrast, HEPA-1 (Figure 8A), PC-12 (not shown), and HMEC (not shown) exhibited only minimal increases at high particle concentrations. Rhod-2 fluorescence showed an even more striking difference between RAW 264.7 and BEAS-2B cells, with the former cell type showing a robust increase in $[Ca^{2+}]_m$ at particle doses >25 μg/mL, while the latter cell mounted only a weak response at the highest particle concentration (Figure 8B). HEPA-1, PC-12, and HEMC did not exhibit an increase in $[Ca^{2+}]_m$.

Since the foregoing data suggest that mitochondrial calcium uptake could play a critical role in the observed toxicity in RAW 264.7 and BEAS-2B cells, we as-

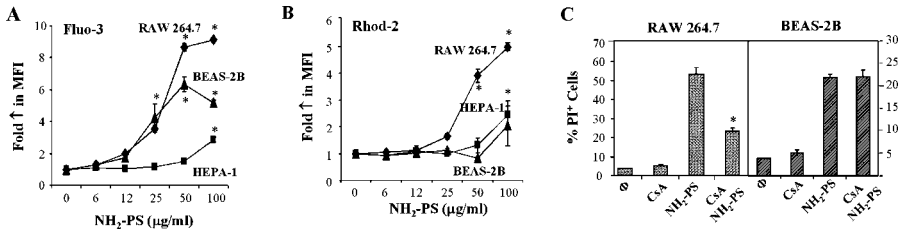

Figure 8. Flow cytometry analysis showing differential effect of NH_2-PS on cytosolic and mitochondrial calcium levels, including the CsA effect on cellular viability. (A) Comparison of the cytosolic Ca^{2+} levels in cells treated with the indicated amount of NH_2-PS for 6 h as detected by Fluo-3 fluorescence. (B) Comparison of the mitochondrial Ca^{2+} levels using Rhod-2 in a similar experiment. (C) PI uptake comparing the cytotoxicity of NH_2-PS in RAW 264.7 and BEAS-2B cells in the presence or absence of CsA. The cells were pretreated with 2 μM CsA, followed by exposure to 25 μg/mL of NH_2-PS for 6 h. Data are representative of three separate experiments. *$p < 0.01$, compared to NH_2-PS.

sessed the effect of cyclosporine A (CsA) on cell death. CsA interferes in the ability of the Ca^{2+}-dependent PTP regulator, cyclophilin D,[19–21] to engage in pore opening.[19] PI uptake studies reveal that, while CsA was capable of a significant reduction of NH_2-PS cytotoxicity in RAW 264.7 cells, this drug had no protective effects in BEAS-2B cells (Figure 8C). These data suggest that, while intracellular Ca^{2+} release plays a role in initiating cellular apoptosis in RAW 264.7 cells (Figure 2), mitochondrial damage in BEAS-2B cells proceeds independent of Ca^{2+}-triggered PTP opening. This finding is compatible with the lack of caspase activation and DNA cleavage in the latter cell type (Figure 2). However, rapid ATP depletion, $\Delta\Psi_m$ decline, and ultrastructural changes in BEAS-2B indicate that mitochondria are involved in particle toxicity. Since we have previously shown that ambient ultrafine particles damage and lodge in mitochondria, we asked whether FITC-NPs colocalize with mitochondria. This was accomplished by performing fluorescence staining for the complex V inhibitor protein, as described in Figure S11A. No particle colocalization with mitochondria could be seen in either RAW 264.7 or BEAS-2B cells (Figure S11B). Thus, although NH_2-PS induces mitochondrial damage in BEAS-2B cells, this utilizes an unknown mitochondrial route that is downstream from caveolar uptake.

Cationic PS Nanoparticles Induce Pulmonary Inflammation in Mice. In order to determine whether neutral, NH_2-PS, or COOH-PS nanospheres induce similar responses in the intact lung as in tissue culture cells, 100 μg of each particle type was administered by intratracheal instillation for 16 h, followed by bronchoalveolar lavage (BAL). The BAL fluid was analyzed for total protein content, LDH levels, and cell counts as described in our previous publication[22] (Figure 9). NH_2-PS induced significantly more protein in the BAL fluid than the other particle types (Figure 9A). Similarly, NH_2-PS induced a significant increase in LDH levels compared to the other particle types, which nonetheless did induce significant changes themselves (Figure 9B). While all the particle types did induce an increase in BAL cell counts, the increases in the total, macrophage, and neutrophil cell counts were significantly higher for NH_2-PS compared to COOH-PS or PS (Figure 9C). This experiment provides proof-of-principle that inhalation exposures could possibly lead to adverse health outcomes, as demonstrated by the clinical experience of the development of acute pulmonary edema and inflammation in spray paint workers exposed to cationic polymeric particles.[10]

DISCUSSION

In this study we compared cationic particle effects in five different cell types that represent portal-of-entry (macrophages and epithelium) or systemic (HEPA-1, HMEC, and PC-12) cellular targets for engineered NPs. Although NH_2-PS nanospheres were highly toxic in RAW 264.7 and BEAS-2B cells, HMEC, HEPA-1, and PC-12 cells were relatively resistant to this damage. These differences may lie in the innate nature of these cells types, since macrophages and lung epithelial cells possess distinctive first-line-of-defense features in the pulmonary milieu compared to the other cell types. This

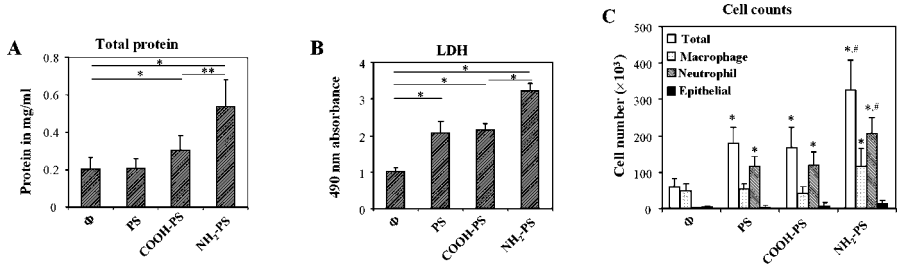

Figure 9. Differential pulmonary toxicity in Balb/c mice receiving intratracheal instillation of 100 μg/mL of particles for 16 h. (A) Total protein content in bronchoalveolar lavage fluid (BALF) was detected using the Bradford method. (B) LDH content in BALF was detected using an LDH detection kit as described in Materials and Methods. (C) Differential cell counts as expressed for total number of cells, macrophages, neutrophils, and epithelial cells. Data are representative of two separate experiments. *$p < 0.01$ and **$p < 0.05$ compared to control. #$p < 0.05$ compared with other particle types.

TABLE 2. Summary of Cellular Events in Response to NH_2-PS Nanospheres[a]

cell	uptake	lysosomal permeability	↑ $[Ca^{2+}]_i$	↑ $[Ca^{2+}]_m$	↓ $\Delta\Psi_m$	ATP	cell death	inhibitors
RAW264.7	LAMP-1$^+$ endosome	+++	+++	+++	+++	+++	apoptosis	BFA CsA
BEAS-2B	caveolae	−	++	−	++	+++	necrosis	MbCD
HMEC	LAMP-1$^+$ endosome	−	−	−	−	−	cytotoxic at high dose only	none
HEPA-1	LAMP-1$^+$ endosome	−	−	−	−	−	cytotoxic at high dose only	none
PC-12	?	−	−	−	−	−	−	none

[a]The number of plus signs is a semiquantitative measure according to which + refers to 5–33% value of highest cellular responses, ++ to 33–66%, and +++ to >66%. A <5% value change was considered as equivocal (−).

is compatible with our findings that these two cell lines exhibited a high potential toward superoxide generation and $[Ca^{2+}]_i$ flux upon cationic particle exposure compared to other cell types. While the cell death pathway in RAW 264.7 cells is apoptotic in nature, the cytotoxic response in BEAS-2B cells proceeded independent of caspase activation. Using fluorescent-labeled NH_2-PS, we followed the routes of particle uptake and possible relationship to cellular damage. Confocal microscopy showed that the cationic particles entered a LAMP-1 positive compartment in RAW 264.7 cells, from which the particles could escape by inducing lysosomal rupture. A proton pump inhibitor could interfere in this pathway. Subsequent deposition of the particles in a non-lysosomal compartment induced an increase in cytosolic and mitochondrial Ca^{2+} flux that could be linked to cytotoxicity based on sensitivity to CsA. In contrast, NH_2-PS toxicity in BEAS-2B cells did not require lysosomal processing, stimulation of proton pump activity, or an increase in $[Ca^{2+}]_m$. Instead, in these cells the particles were taken up by caveolae, and their toxicity could be disrupted by removal of membrane cholesterol with cyclodextrin. Although the cationic particles induced mitochondrial damage, ATP depletion, and cytotoxicity in BEAS-2B cells, CsA did not affect cell death. While cationic particles were taken up in a LAMP-1 positive compartment in HEPA-1 cells, this did not lead to lysosomal permeabilization, increased Ca^{2+} flux, mitochondrial damage, or cell death. A similar lack of toxicity and failure to interfere in mitochondrial function was seen in HMEC and PC-12 cells. All considered, these data show cell-specific differences in cationic PS nanoparticle processing and toxicity, which are summarized in Table 2.

There is growing recognition that endocytosis plays a fundamental role in the regulation of a wider range of cellular functions.[23] As demonstrated in this study, cationic NP uptake by endosomes has an effect on proton pump activity, intracellular Ca^{2+} flux, and mitochondrial function. While it is beyond the scope of this article to discuss in detail all the biological pathways associated with particle endocytosis, it is worth considering the importance of the lysosome in RAW 264.7 cytotoxicity. The cationic charge on the particle surface is likely responsible for the initial binding to the surface membrane, as suggested by previous findings that polyamine-PS microparticles engage in strong ionic interactions with the negatively charged cell membrane.[24] Particle uptake by this mechanism is dependent on primary particle size, since 200 (Figure 1) and 600 nm cationic PS microspheres[9] lacked the toxicity of the 60 nm particles. Once inside the lysosomal compartment, the NH_2 group on the particle surface is thought to perturb proton pump activity. According to the proton sponge hypothesis, the high H^+ buffering capacity of titratable amines (such as NH_2) could interfere in endosomal acidification.[13,14] This leads to exaggerated proton pump activity, osmotic swelling, and ultimately the rupture of the lysosome. This explains the interference in particle relocation and cytotoxicity by BFA (Figure 5). In contrast, non-titratable polyamines that exhibit a fixed positive charge (*e.g.*, amidine) function less efficiently as a proton sponge, which could explain why amidine substitution on the particle surface was less toxic (Figure S2).

How does lysosomal rupture lead to apoptosis? A number of cell death pathways have been linked to lysosomal leakage, including leakage of lysosomal enzymes that truncate Bid or activate Bax, activate phospholipases, activate pro-caspases, or damage the mitochondrial outer membrane, leading to the release of cytochrome *c* and other pro-apoptotic factors.[25,26] This is in accordance with previous demonstrations that an increase in lysosomal pH is capable of interfering in the apoptogenic effects of some lysosomotropic agents.[27,28] Alternatively, the released cationic NP could target mitochondria or other cellular organelles such as the endoplasmic reticulum (ER) directly. In RAW 264.7 cells, we demonstrated that the cationic NPs induced an increase in $[Ca^{2+}]_i$ and $[Ca^{2+}]_m$ and that CsA could interfere in cytotoxicity (Figure 8). These findings suggest that the mitochondrial response could be triggered by the increase in $[Ca^{2+}]_i$. In the attempt to buffer this increase, the rise in $[Ca^{2+}]_m$ could exceed the PTP threshold, thereby triggering the release of pro-apoptotic factors.[19–21] Once a single mitochondrion undergoes large-scale PTP opening, this could trigger a wave of Ca^{2+} release events that spread through the cell, leading to progressively more mitochondrial involvement.[19–21] Damage to the mitochondrial inner membrane could increase ROS production that causes further lysosomal disruption.[27] Taken together, these

data suggest that crosstalk between the lysosome and mitochondria could play an important role in determining apoptosis in RAW 264.7 cells. It is possible that the ER may be involved in this event because of its close interaction with the mitochondrion in maintaining cellular Ca^{2+} homeostasis and apoptosis.[29,30]

How do we explain BEAS-2B toxicity, which is characterized by prominent mitochondrial damage but no sign of caspase activation (Figures 2 and 7)? Confocal microscopy demonstrated that the fluorescent-labeled particles co-localize with caveolae and that disruption of these cholesterol-rich membrane domains prevents particle uptake and cytotoxicity (Figure 6). This suggests that caveolae play a role in cytotoxicity (Figures 6 and 7). It has previously been shown that caveolae affect cellular viability by interfering in cellular proliferation signals.[31] It is also known that caveolae affect intracellular Ca^{2+} flux and mitochondrial function.[32,33] For instance, caveolin-1 is an inhibitor of platelet-derived growth factor growth signals, which are involved in the regulation of cellular apoptosis at the mitochondrial level.[32] Caveolin-1 also increases sensitivity to apoptosis induction by bromocriptine in pituitary adenoma GH3 cells.[34] In addition, caveolin-1 associates with molecules that are crucial for Ca^{2+} handling, including voltage-dependent calcium channels and the ER protein, calreticulin.[35] These results suggest that caveolae and the ER form a functional unit that could contribute to the regulation of the $[Ca^{2+}]_i$. The ER itself is composed of multiple domains, among which the smooth ER (SER) interacts with mitochondria to regulate Ca^{2+} sequestration and apoptosis.[30] Moreover, mitochondria associate directly and are in close communication with the ER.[30] It is noteworthy that we did not observe evidence of caspase activation in BEAS-2B cells, in spite of the fact that that NH_2-PS leads to increased $[Ca^{2+}]_i$, mitochondrial damage, ATP depletion, and cytotoxicity (Figures 1, 2, 7,and 8). Mitochondrial damage in these cells is characterized by initial mitochondrial condensation. While the significance of mitochondrial condensation is unknown, this phenomenon has previously been shown to coincide with a decrease in $\Delta\Psi_m$ and cellular ATP levels during cellular injury by activated complement components and exotoxin A.[36,37] The proposed basis of this injury includes damage to the mitochondrial membrane that is responsible for K^+ and H_2O loss. Although this could be due to direct particle contact with a mitochondrion, we did not observe direct colocalization of the FITC-NP with mitochondria (Figure S11).

It is worth mentioning that, in the growing literature dealing with gene, DNA, and plasmid delivery by cationic polymers (polyplexes) and cationic lipids (lipoplexes), it has been reported that the uptake and processing of these microsized delivery systems depend on acidifying lysosomes and caveolae.[38–41] Moreover, it is known that many of these non-viral transfection systems can induce cellular toxicity and apoptosis based on their cationic charge and interference in proton pump activities.[13,15,38] It has also been reported with polyplexes prepared from the cationic polymer, polyethyleneimine, that there are cell-dependent variations in endocytosis, perturbation of the proton pump, and induction of toxicity.[39–42] Depending on the dominant mechanism of cellular uptake, it was demonstrated that it is possible to interfere in polyplex uptake by inhibitors of the caveolae-dependent pathway as well as the use of bafilomycin A1.[39–41]

Interestingly, the cationic PS nanospheres had no effect on cellular toxicity in HEPA-1, HMEC, and PC-12 cells (Figure 1). Although the cationic particles entered a LAMP-1 compartment in HMEC and HEPA-1 cells, no lysosomal permeabilization could be detected in these cells (Figure 5A). While we have no explanation for these differences at present, these data serve to demonstrate the cell-specific nature of particle toxicity.

Finally, it is appropriate to comment on the importance of these findings for nanotoxicology. While no clinical NP toxicity has been reported to date, it is interesting that cationic spray paint particles are capable of inducing pulmonary toxicity in an occupational setting (Ardystil syndrome).[10] This serves as a warning that other engineered NPs that carry a positive surface charge may cause similar adverse health effects. This notion is further bolstered by the increased pulmonary toxicity of cationic PS in mice receiving intratracheal particles (Figure 9). While intratracheal instillation does not provide real-life exposure, the use of this approach is to provide proof-of-principle that cationic particle deposition in the lung can lead to injury while naked or anionic particles have little effect. This is useful data from the perspective that the injury profile in the lung is reflective of the injury profile at the cellular level. This also magnifies the importance of ultimately performing inhalation studies to demonstrate that aerosolized inhalation indeed does lead to toxicity, similar to what is seen in the Ardystil syndrome in humans. We propose that screening for NP toxicity should include an assessment of particle charge, in addition to other physicochemical characterizations. At this stage it appears that detection of lysosomal permeabilization, mitochondrial function, cellular ATP levels, and $[Ca^{2+}]_i$ could be valuable biological screening tools in addition to determining the zeta potential of the particles. We have previously demonstrated that a screening paradigm for cellular oxidative stress and ROS generation is capable of discerning cationic particle toxicity-based ROS production by damaged mitochondria.[9] This suggests that we should supplement this biological screening system with assays for lysosomal function, cellular ATP content, and intracellular Ca^{2+} flux. Doing so could provide us with a high-throughput system that can be used to screen for potential toxicity of a large number of NMs simultaneously.

CONCLUSIONS

We demonstrate that cationic particles exert differential toxicity in five different cell lines. RAW 264.7 (macrophage) and BEAS-2B (epithelial) cells were very sensitive to NH_2-PS, while HMEC (human microvascular endothelial), HEPA-1 (hepatoma), and PC-12 cells (pheochromocytoma) were relatively resistant to particle injury. Cationic particle-induced cell death in RAW 264.7 and BEAS-2B cells differed in nature, presenting apoptotic and necrotic features, respectively. Moreover, RAW 264.7 cells used an endosomal−lysosomal route of uptake, while BEAS-2B cells used a caveolar uptake mechanism. The two distinct processing routes result in different functional and structural mitochondrial changes that precede the onset of cell death in these two cell lines.

MATERIALS AND METHODS

Chemicals and Nanoparticles. Propidium iodide (PI), bafilomycin A1 (BFA), concanamycin A, fluorescein isothiocynate (FITC), succinic anhydride, and fluorescamine were from Sigma (St. Louis, MO). 5,5′,6,6′-Tetrachloro-1,1′,3,3′-tetraethylbenzimidazolylcarbocyanine iodide/chloride (JC-1), acridine orange (AO), 1-amino-5-(2,7-dichloro-6-acetomethoxy-3-oxo-3*H*-xanthen-9-yl)phenoxy]-2-(2′-amino-5′-methylphenoxy)ethane-*N*,*N*,*N*′,*N*′-tetraacetic acid, pentaacetoxy methyl ester (Fluo-3), 1-[2-amino-5-(3-dimethylamino-6-dimethylammonio-9-xanthenyl)phenoxy]-2-(2-amino-5-methylphenoxy)]ethane-*N*,*N*,*N*′,*N*′-tetraacetic acid, tetraacetoxy methyl ester (Rhod-2), MitoSOX red, and Alexa 594-labeled secondary antibodies were obtained from Molecular Probes (Eugene, OR). The MTS assay kit and ATPLite 1Step reagents were obtained from Perkin-Elmer (Waltham, MA). Dulbecco's Modified Eagle's Medium (DMEM), penicillin/streptomycin, L-glutamine, and 200 nm fluorescent FITC-modified polystyrene (PS) particles were purchased from Invitrogen (Carlsbad, CA). Fetal bovine serum (FBS) was from Atlanta Biologicals, Inc. (Lawrenceville, GA). Rat anti-mouse monoclonal to lysosomal membrane glycoprotein 1 (LAMP-1, 1D4B) and mouse anti-human monoclonal (H4A3) were bought from Abcam (Cambridge, MA). Rabbit anti-caveolin-1 polyclonal antibody was bought from BD Biosciences Pharmingen (San Jose, CA). PS)nano- and microspheres were obtained from Bangs Laboratory (Fishers, IN). These include 60 nm unmodified (PS), 60 nm carboxylated (COOH-PS), and 60 nm amino-modified (NH_2-PS) polystyrene particles. For all experiments and analyses, water was deionized and filtered with a 0.45 μm pore size polycarbonate syringe filter (Millipore, Billerica, MA). All chemicals were reagent grade and used without further purification or modification.

Physicochemical Characterization. All NPs were characterized for size, size distribution, shape, and charge (Table 1). NP shape and structure were characterized using a transmission electron microscope (JEM 2010, JEOL USA, Inc., Peabody, MA). Microfilms for TEM imaging were made by placing a drop of the respective NP suspension onto a 200-mesh copper TEM grid (Electron Microscopy Sciences, Washington, PA) and then drying at room temperature overnight. A minimum of five images of each sample were collected to obtain representative views.

Particle size distribution (PSD) was evaluated using a ZetaPALS (Brookhaven Instruments Corp., Holtsville, NY). This instrument measures the dynamic light scattering (DLS) from a suspension at an angle of 90°. It is capable of measuring particles in the size range from 2 nm to 2 μm. Size measurements were performed on dilute NP suspensions in aqueous solution at pH 7.0 or complete cell culture media at pH 7.4. The ZetaPALS was also used to measure the electrophoretic mobility of the NPs suspended in solution. Electrophoretic mobility is used as an approximation of particle surface charge and can be used to calculate zeta potential. The Helmholtz−Smoluchowski equation was used to correlate electrophoretic mobility to zeta potential. The PSD and electrophoretic mobility of all NPs were also measured in the complete culture media for comparison.[9]

Cell Culture and Co-incubation with Nanoparticles. All cell cultures were maintained in 25 cm^2 cell culture flasks, in which the cells were passaged at 70–80% confluency every 2–4 days. RAW 264.7 and HEPA-1 cell lines were cultured in DMEM containing 10% fetal calf serum (FCS), 100 U/mL penicillin, 100 μg/mL streptomycin, and 2 mM L-glutamine (complete medium). BEAS-2B cells were cultured in bronchial epithelial growth medium (Clonetics, San Diego, CA) in type I rat tail collagen-coated flasks or plates. HMEC cells were cultured in MCDB131 medium (Sigma, St. Louis, MO) supplemented with 10% (v/v) FCS, penicillin/streptomycin (100 units/mL and 100 μg/mL, respectively), 1 mmol/L sodium pyruvate, 90 μg/mL heparin, and 20 μg/mL endothelial cell growth supplement (Fisher Scientific, Waltham, MA). PC12 cells were grown in Dulbecco's Modified Minimal Medium (Hyclone, Logan, UT) supplemented with 5% horse serum (Hyclone), 5% FBS (Hyclone), 100 U/mL penicillin, and 100 μg/mL streptomycin. For exposure to NPs, aliquots of 3×10^5 cells were cultured in 24-well plates in 0.5 mL of medium at 37 °C and 5% CO_2 for the indicated time periods. All the NP solutions were prepared fresh from stock solutions (10 mg/mL) and sonicated for 10 s before addition to cell cultures.

Cell Viability Assay. Cellular viability was determined by the MTS assay, which looks at the reduction of (3-(4,5-dimethylthiazol-2-yl)-5-(3-carboxymethoxyphenyl)-2-(4-sulfophenyl)-2*H*-tetrazolium (MTS) to formazan in viable cells.[43] Briefly, 50×10^3 cells were plated onto 96 multiwell plates (Costar, Corning, NY). After incubation with the indicated dose of NPs for various lengths of time at 37 °C, formazan absorbance was measured at 490 nm. The mean absorbance of non-exposed cells was the reference value for calculating 100% cellular viability.

Cellular Staining with Fluorescent Probes and Flow Cytometry. Cells were stained with the fluorescent dyes diluted in DMEM. The following dye combinations were added for 15–30 min at 37 °C in the dark: (i) 47.5 μg/mL PI in 200 μL of DMEM (assessment of cell death); (ii) 5 μM DyeCycle Orange (assessment of DNA cleavage during apoptosis); (iii) 50 μM D2R trifluoroacetate (assessment of caspase activation); (iv) 5 μM JC-1 (assessment of $\Delta\Psi_m$); (v) 5 μM Fluo-3 (assessment of cytoplasmic free calcium); (vi) 4 μM Rhod-2 (assessment of mitochondrial free calcium); and (vii) 5 μg/mL AO (assessment of lysosomal integrity). Flow cytometry was performed using a FACScan or LSR instrument (Becton Dickinson, Mountain View, CA) equipped with a single 488 nm argon laser. Fluo-3 and D2R fluorescence was analyzed in the FL-1 channel, while PI, DyeCycle Orange, and Rhod-2 fluorescence was analyzed in FL-2. AO was analyzed in FL-3, and JC-1 was analyzed in both FL-1 and FL-2. Forward and side scatter were used to gate out cellular fragments.[44,45]

Transmission Electron Microscopy. Harvested cells were fixed with 2.5% glutaraldehyde in 0.1 M phosphate-buffered saline (PBS) and washed. After post-fixation in 1% OsO_4 in PBS for 1 h, the cells were dehydrated in a graded series of ethanol, treated with propylene oxide, and embedded in Epon. Approximately 60–70 nm thick sections were cut on a Reichert-Jung Ultracut E ultramicrotome and picked up on Formvar-coated copper grids. The sections were stained with uranyl acetate and Reynolds lead citrate and examined on a JEOL 100CX electron microscope at 80 kV in the UCLA BRI Electron Microscopy Core.

Surface Modification of NH_2-PS. The amino groups on the cationic particle surfaces were converted into carboxylates by reaction with succinic anhydride.[46] First, 0.5 mg of succinic anhydride was dissolved in 1 mL of carbonate buffer (pH 9.1). Next, 100 μL of the NH_2-PS suspension (100 mg/mL) was added to the basic succinic anhydride solution and stirred for 12 h. The mixture was dialyzed against filtered, deionized water at room temperature to remove the excess salt and unreacted compounds. A fluorescamine assay was used to determine the efficiency of converting the primary amines in the NH_2-PS into carboxylate

groups.[47] Equal amounts of fluorescamine solution were added to dilute suspensions of NH_2-PS and succinylated-NH_2-PS. The bright green color that was observed in the suspension of NH_2-PS upon the addition of fluorescamine confirmed the presence of the amine groups. By contrast, the faint green color that was observed in the suspension of succinylated-NH_2-PS indicated that most of the surface primary amines had been converted into the carboxylate groups.

Fluorescence Labeling of NH_2-PS. A total of 0.5 mL of NH_2-PS (100 mg/mL suspension) was mixed with 1 mL of carbonate buffer solution (pH 9.1). First, 5 mg of FITC was dissolved in 100 μL of dimethyl sulfoxide (DMSO) and mixed with 400 μL of carbonate buffer before being added to the NH_2-PS solution. After the mixture was stirred for 24 h in the dark, the unreacted FITC molecules were quenched with ammonium chloride. To remove DMSO and unreacted FITC, the solution was dialyzed (Fisher brand, 12 000–14 000 MW cutoff) against filtered, deionized water. The water was consistently replaced and the dialysis continued until complete removal of unreacted FITC molecules.

Immunocytochemistry and Confocal Microscopy. Cultured cells on chamber slides were fixed, permeabilized, and labeled with a standard immunocytochemistry protocol. LAMP-1 staining was performed by using 1:500 dilutions of a rat anti-mouse (1D4B) or mouse antihuman monoclonal antibodies (H4A3), followed by an Alexa 594-labeled secondary antibody. Caveolin-1 was labeled with a primary rabbit anti-caveolin polyclonal antibody for 1 h at room temperature, followed by the addition of a 1:500 dilution of secondary Alexa-594-conjugated goat anti-rabbit IgG for 1 h at room temperature. Cell membranes were stained with 5 μg/mL wheat germ agglutinin−Alexa Fluor 594 conjugate in PBS for 30 min. Slides were mounted in Prolong antifade medium with DAPI (Molecular Probes, Eugene, OR) and visualized under a confocal microscope (Leica Confocal 1P/FCS).

Fluorescent microscopy was performed with a Leica TCS-SP confocal microscope at the CNSI Advanced Light Microscopy/Spectroscopy Shared Facility at UCLA. High-magnification images were obtained with a 63× objective. Optical sections were averaged 2–4 times to reduce noise. Images were processed using Leica Confocal Software. Co-localization of labeled NPs with LAMP-1 and caveolin-1 was quantified by the Image J Colocalization Analysis Software from the NIH.[48]

Assessment of Lysosomal Integrity by Acridine Orange (AO) Release. Cells were exposed to 5 μg/mL AO in DMEM plus horse serum (complete medium) for 15 min at 37 °C. After rinsing of the cells in complete medium and culturing at 37 °C for 4 h, orange fluorescence intensity was determined by flow cytometry in the FACScan using the FL3 channel.[49] CELLQUEST software was used to analyze flow cytometry, and the results were presented as the percentage of cells with low AO fluorescence intensity (AO^{low}).

Determination of Cellular ATP Content. The cellular ATP content was determined by using the ATPlite firstep kit that uses firefly luciferase to provide a linear increase in luminescence with increased cell number. Luminescence was recorded using a Moonlight 2010 luminometer.

Intratracheal Instillation of Nanaoparticles. Animal experiment protocols were reviewed and approved by the The Chancellor's Animal Research Committee (ARC) at UCLA. Animal experiments were performed in accordance with UCLA guidelines for care and treatment of laboratory animals and the NIH Guide for the Care and Use of Laboratory Animals in Research (DHEW78-23). We used 100 μg particles for intratracheal instillation in anesthesized Balb/c mice. We used six mice per group, since this number has enough statistical power to discern differences in the toxic responses. Animals were sacrificed 16 h later to obtain bronchoalveolar lavage fluid (BALF) for analysis of pro-inflammatory and cytotoxicity markers, as previously described by us.[22] BALF was used to obtain total and differential cell counts, as well as to measure LDH and protein content.

Acknowledgment. Funding for this study was provided by the U.S. Public Health Service Grants, U19 AI070453, RO1 ES10553, RO1 ES10253, and RO1 ES015498, as well as the U.S. EPA STAR award (RD-83241301) to the Southern California Particle Center. This work is also supported by the UC Lead Campus for Nanotoxicology Training and Research, funded by UC TSR&TP. Fluorescent microscopy was performed at the CNSI Advanced Light Microscopy/Spectroscopy Shared Facility at UCLA. This work has not been subjected to the EPA for peer and policy review.

Supporting Information Available: Histogram to show PI uptake in RAW 264.7 cells (Figure S1), time course of NH_2-PS induced toxicity and comparison of the toxicity of amidine vs NH_2 substitution on the PS nanoparticle surface in RAW 264.7 cells (Figure S2), interpretation of the assays for caspase activation, DNA degradation and mitochondrial membrane potential (Figure S3), comparison of caspase activation, DNA degredation, mitochondrial membrane potential and ATP content as markers for apoptosis and necrosis (Figure S4), TEM of the NH_2-PS and FITC-NH_2-PS particles and measurement of the zeta potential (Figure S5), comparison of the toxicity of NH_2-PS vs FITC-labeled NH_2-PS (Figure S6), subcellular localization of FITC-NH_2-PS in RAW 264.7 cells (Figure S7), confocal microscopy to study the subcellular localization of FITC-NH_2-PS (Figure S8), assessment of the lysosomal permeabilization (Figure S9), TEM of RAW 264.7 ultrastructure (Figure S10), confocal microscopy of intracellular localization of FITC-NH_2-PS in comparison with the mitochondria (Figure S11). This material is available free of charge *via* the Internet at http://pubs.acs.org.

REFERENCES AND NOTES

1. Nel, A.; Xia, T.; Madler, L.; Li, N. Toxic Potential of Materials at the Nanolevel. *Science* **2006**, *311*, 622–627.
2. Colvin, V. L. The Potential Environmental Impact of Engineered Nanomaterials. *Nat. Biotechnol.* **2003**, *21*, 1166–1170.
3. Donaldson, K.; Stone, V.; Tran, C. L.; Kreyling, W.; Borm, P. J. Nanotoxicology. *Occup. Environ. Med* **2004**, *61*, 727–728.
4. Oberdorster, G.; Oberdorster, E.; Oberdorster, J. Nanotoxicology: An Emerging Discipline Evolving from Studies of Ultrafine Particles. *Environ. Health Perspect.* **2005**, *113*, 823–839.
5. Service, R. F. Nanotoxicology. Nanotechnology Grows Up. *Science* **2004**, *304*, 1732–1734.
6. The Royal Society and The Royal Academy of Engineering. Nanoscience and nanotechnologies: opportunities and uncertainties. Report, July 29, 2004; The Royal Society: London, 2004 (www.royalsoc.ac.uk/policy).
7. Linse, S.; Cabaleiro-Lago, C.; Xue, W. F.; Lynch, I.; Lindman, S.; Thulin, E.; Radford, S. E.; Dawson, K. A. Nucleation of Protein Fibrillation by Nanoparticles. *Proc. Natl. Acad. Sci. U.S.A.* **2007**, *104*, 8691–8696.
8. Oberdorster, G.; Maynard, A.; Donaldson, K.; Castranova, V.; Fitzpatrick, J.; Ausman, K.; Carter, J.; Karn, B.; Kreyling, W.; Lai, D.; *et al. Part. Fibre Toxicol.* **2005**, *2*, 8.
9. Xia, T.; Kovochich, M.; Brant, J.; Hotze, M.; Sempf, J.; Oberley, T.; Sioutas, C.; Yeh, J. I.; Wiesner, M. R.; Nel, A. E. Comparison of the Abilities of Ambient and Manufactured Nanoparticles to Induce Cellular Toxicity According to an Oxidative Stress Paradigm. *Nano Lett.* **2006**, *6*, 1794–1807.
10. Hoet, P. H.; Gilissen, L.; Nemery, B. Polyanions Protect Against the In Vitro Pulmonary Toxicity of Polycationic Paint Components Associated with the Ardystil Syndrome. *Toxicol. Appl. Pharmacol.* **2001**, *175*, 184–190.
11. Nemmar, A.; Hoylaerts, M. F.; Hoet, P. H.; Vermylen, J.; Nemery, B. Size Effect of Intratracheally Instilled Particles on Pulmonary Inflammation and Vascular Thrombosis. *Toxicol. Appl. Pharmacol.* **2003**, *186*, 38–45.
12. Chen, C. Z.; Cooper, S. L. Interactions Between Dendrimer Biocides and Bacterial Membranes. *Biomaterials* **2002**, *23*, 3359–3368.
13. Boussif, O.; Lezoualc'h, F.; Zanta, M. A.; Mergny, M. D.; Scherman, D.; Demeneix, B.; Behr, J. P. A Versatile Vector for Gene and Oligonucleotide Transfer into Cells in Culture and In Vivo: polyethylenimine. *Proc. Natl. Acad. Sci. U.S.A.* **1995**, *92*, 7297–7301.
14. Sonawane, N. D.; Thiagarajah, J. R.; Verkman, A. S. Chloride Concentration in Endosomes Measured Using a Ratioable Fluorescent Cl- Indicator: Evidence for Chloride Accumulation During Acidification. *J. Biol. Chem.* **2002**, *277*, 5506–5513.

15. Asokan, A.; Cho, M. J. Exploitation of Intracellular pH Gradients in the Cellular Delivery of Macromolecules. *J. Pharm. Sci.* **2002**, *91*, 903–913.
16. Hug, H.; Los, M.; Hirt, W.; Debatin, K. M. Rhodamine 110-Linked Amino Acids and Peptides as Substrates To Measure Caspase Activity upon Apoptosis Induction in Intact Cells. *Biochemistry* **1999**, *38*, 13906–13911.
17. Kirkham, M.; Parton, R. G. Clathrin-independent Endocytosis: New Insights into Caveolae and Non-caveolar Lipid Raft Carriers. *Biochim. Biophys. Acta* **2005**, *1746*, 349–363.
18. Sieczkarski, S. B.; Whittaker, G. R. Dissecting Virus Entry via Endocytosis. *J. Gen. Virol.* **2002**, *83*, 1535–1545.
19. Halestrap, A. P.; McStay, G. P.; Clarke, S. J. The Permeability Transition Pore Complex: Another View. *Biochimie* **2002**, *84*, 153–166.
20. Kim, J. S.; He, L.; Lemasters, J. J. Mitochondrial Permeability Transition: A Common Pathway to Necrosis and Apoptosis. *Biochem. Biophys. Res. Commun.* **2003**, *304*, 463–470.
21. Kroemer, G.; Galluzzi, L.; Brenner, C. Mitochondrial Membrane Permeabilization in Cell Death. *Physiol. Rev.* **2007**, *87*, 99–163.
22. Hao, M.; Comier, S.; Wang, M.; Lee, J. J.; Nel, A. Diesel Exhaust Particles Exert Acute Effects on Airway Inflammation and Function in Murine Allergen Provocation Models. *J. Allergy Clin. Immunol.* **2003**, *112*, 905–914.
23. Polo, S.; Di Fiore, P. P. Endocytosis Conducts the Cell Signaling Orchestra. *Cell* **2006**, *124*, 897–900.
24. Hong, S.; Leroueil, P. R.; Janus, E. K.; Peters, J. L.; Kober, M. M.; Islam, M. T.; Orr, B. G.; Baker, J. R., Jr.; Banaszak Holl, M. M. Interaction of Polycationic Polymers with Supported Lipid Bilayers and Cells: Nanoscale Hole Formation and Enhanced Membrane Permeability. *Bioconjugate Chem.* **2006**, *17*, 728–734.
25. Reiners, J. J., Jr.; Caruso, J. A.; Mathieu, P.; Chelladurai, B.; Yin, X. M.; Kessel, D. Release of Cytochrome c and Activation of Pro-caspase-9 Following Lysosomal Photodamage Involves Bid Cleavage. *Cell Death Differ.* **2002**, *9*, 934–944.
26. Bidere, N.; Lorenzo, H. K.; Carmona, S.; Laforge, M.; Harper, F.; Dumont, C.; Senik, A. Cathepsin D Triggers Bax Activation, Resulting in Selective Apoptosis-Inducing Factor (AIF) Relocation in T Lymphocytes Entering the Early Commitment Phase to Apoptosis. *J. Biol. Chem.* **2003**, *278*, 31401–31411.
27. Terman, A.; Kurz, T.; Gustafsson, B.; Brunk, U. T. Lysosomal Labilization. *IUBMB Life* **2006**, *58*, 531–539.
28. Terman, A.; Gustafsson, B.; Brunk, U. T. The Lysosomal-Mitochondrial Axis Theory of Postmitotic Aging and Cell Death. *Chem. Biol. Interact.* **2006**, *163*, 29–37.
29. Szabadkai, G.; Simoni, A. M.; Bianchi, K.; De, S. D.; Leo, S.; Wieckowski, M. R.; Rizzuto, R. Mitochondrial Dynamics and Ca2+ Signaling. *Biochim. Biophys. Acta* **2006**, *1763*, 442–449.
30. Rizzuto, R.; Pozzan, T. Microdomains of Intracellular Ca^{2+}: Molecular Determinants and Functional Consequences. *Physiol. Rev.* **2006**, *86*, 369–408.
31. Drab, M.; Verkade, P.; Elger, M.; Kasper, M.; Lohn, M.; Lauterbach, B.; Menne, J.; Lindschau, C.; Mende, F.; Luft, F. C.; *et al.* Loss of Caveolae, Vascular Dysfunction, and Pulmonary Defects in Caveolin-1 Gene-disrupted Mice. *Science* **2001**, *293*, 2449–2452.
32. Peterson, T. E.; Guicciardi, M. E.; Gulati, R.; Kleppe, L. S.; Mueske, C. S.; Mookadam, M.; Sowa, G.; Gores, G. J.; Sessa, W. C.; Simari, R. D. Caveolin-1 Can Regulate Vascular Smooth Muscle Cell Fate by Switching Platelet-derived Growth Factor Signaling from a Proliferative to an Apoptotic Pathway. *Arterioscler. Thromb. Vasc. Biol.* **2003**, *23*, 1521–1527.
33. Goetz, J. G.; Nabi, I. R. Interaction of the Smooth Endoplasmic Reticulum and Mitochondria. *Biochem. Soc. Trans.* **2006**, *34*, 370–373.
34. Jiang, Y. N.; Li, Y. H.; Ke, M. W.; Tseng, T. Y.; Tang, Y. B.; Huang, M. C.; Cheng, W. T.; Ju, Y. T. Caveolin-1 Sensitizes Rat Pituitary Adenoma GH3 Cells to Bromocriptine Induced Apoptosis. *Cancer Cell Int.* **2007**, *7*, 1.
35. Daniel, E. E.; El-Yazbi, A.; Cho, W. J. Caveolae and Calcium Handling, a Review and a Hypothesis. *J. Cell Mol. Med.* **2006**, *10*, 529–544.
36. Plotkowski, M. C.; Povoa, H. C.; Zahm, J. M.; Lizard, G.; Pereira, G. M.; Tournier, J. M.; Puchelle, E. Early Mitochondrial Dysfunction, Superoxide Anion Production, and DNA Degradation are Associated with Non-Apoptotic Death of Human Airway Epithelial Cells Induced by Pseudomonas Aeruginosa Exotoxin A. *Am. J. Respir. Cell Mol. Biol.* **2002**, *26*, 617–626.
37. Papadimitriou, J. C.; Drachenberg, C. B.; Shin, M. L.; Trump, B. F. Ultrastructural Studies of Complement Mediated Cell Death: A Biological Reaction Model to Plasma Membrane Injury. *Virchows Arch.* **1994**, *424*, 677–685.
38. Akinc, A.; Thomas, M.; Klibanov, A. M.; Langer, R. Exploring Polyethylenimine-mediated DNA Transfection and the Proton Sponge Hypothesis. *J. Gene Med.* **2005**, *7*, 657–663.
39. van der Aa, M. A.; Huth, U. S.; Hafele, S. Y.; Schubert, R.; Oosting, R. S.; Mastrobattista, E.; Hennink, W. E.; Peschka-Suss, R.; Koning, G. A.; Crommelin, D. J. Cellular Uptake of Cationic Polymer-DNA Complexes Via Caveolae Plays a Pivotal Role in Gene Transfection in COS-7 Cells. *Pharm. Res.* **2007**, *24*, 1590–1598.
40. von, G. K.; Sanders, N. N.; Vandenbroucke, R.; De Smedt, S. C.; Wagner, E.; Ogris, M. The Internalization Route Resulting in Successful Gene Expression Depends on Both Cell Line and Polyethylenimine Polyplex Type. *Mol. Ther.* **2006**, *14*, 745–753.
41. Rejman, J.; Bragonzi, A.; Conese, M. Role of Clathrin- and Caveolae-mediated Endocytosis in Gene Transfer Mediated by Lipo- and Polyplexes. *Mol. Ther.* **2005**, *12*, 468–474.
42. Florea, B. I.; Meaney, C.; Junginger, H. E.; Borchard, G. Transfection Efficiency and Toxicity of Polyethylenimine in Differentiated Calu-3 and Nondifferentiated COS-1 Cell Cultures. *AAPS Pharm. Sci.* **2002**, *4*, E12.
43. Wiepz, G. J.; Edwin, F.; Patel, T.; Bertics, P. J. Methods for Determining the Proliferation of Cells in Response to EGFR Ligands. *Methods Mol. Biol.* **2006**, *327*, 179–187.
44. Hiura, T. S.; Li, N.; Kaplan, R.; Horwitz, M.; Seagrave, J. C.; Nel, A. E. The Role of a Mitochondrial Pathway in the Induction of Apoptosis by Chemicals Extracted from Diesel Exhaust Particles. *J. Immunol.* **2000**, *165*, 2703–2711.
45. Li, N.; Venkatesan, M. I.; Miguel, A.; Kaplan, R.; Gujuluva, C.; Alam, J.; Nel, A. Induction of Heme Oxygenase-1 Expression in Macrophages by Diesel Exhaust Particle Chemicals and Quinones Via the Antioxidant-Responsive Element. *J. Immunol.* **2000**, *165*, 3393–3401.
46. Qhobosheane, M.; Santra, S.; Zhang, P.; Tan, W. Biochemically Functionalized Silica Nanoparticles. *Analyst* **2001**, *126*, 1274–1278.
47. Udenfriend, S.; Stein, S.; Bohlen, P.; Dairman, W.; Leimgruber, W.; Weigele, M. Fluorescamine: A Reagent for Assay of Amino Acids, Peptides, Proteins, and Primary Amines in the Picomole Range. *Science* **1972**, *178*, 871–872.
48. Zhou, M.; Schools, G. P.; Kimelberg, H. K. Development of GLAST(+) Astrocytes and NG2(+) Glia in Rat Hippocampus CA1: Mature Astrocytes are Electrophysiologically Passive. *J. Neurophysiol.* **2006**, *95*, 134–143.
49. Yuan, X. M.; Li, W.; Dalen, H.; Lotem, J.; Kama, R.; Sachs, L.; Brunk, U. T. Lysosomal Destabilization in P53-induced Apoptosis. *Proc. Natl. Acad. Sci. U.S.A.* **2002**, *99*, 6286–6291.